Molecular Pharmacology Fast Forward. Published on May 18, 2016 as DOI: 10.1124/mol.115.102731
This article has not been copyedited and formatted. The final version may differ from this version.

Mechanisms of action of novel influenza A/M2 viroporin inhibitors derived from hexamethylene amiloride

Pouria H. Jalily, Jodene Eldstrom, Scott C. Miller, Daniel C. Kwan, Sheldon S. -H. Tai, Doug Chou, Masahiro Niikura, Ian Tietjen, David Fedida

Department of Anesthesiology, Pharmacology, and Therapeutics, Faculty of Medicine, University of British Columbia, Vancouver, British Columbia, Canada (P.H.J, J.E, S.C.M, D.C.K, D.C, I.T, D.F)

Faculty of Health Sciences, Simon Fraser University, Burnaby, British Columbia, Canada (S.S.T, M.N, I.T)

Molecular Pharmacology Fast Forward. Published on May 18, 2016 as DOI: 10.1124/mol.115.102731
This article has not been copyedited and formatted. The final version may differ from this version.

Mechanisms of action of novel influenza A/M2 viroporin inhibitors

Corresponding Author: **Dr. David Fedida**

2.301 Life Sciences Institute, 2350 Health Sciences Mall, Vancouver, BC Canada V6T 1Z3

Telephone: +1 (604) 822 5806, Fax: +1 (604) 822 2281, Email: David.Fedida@ubc.ca

Number of Text Pages: 21

Number of Tables: 3

Number of Figures: 7

Number of References: 37

Number of Words in Abstract: 195

Number of Words in Introduction: 745

Number of Words in Methods: 1591

Number of Words in Results: 4424

Number of Words in Discussion: 1162

Abbreviations

Boc; tert-Butyloxycarbonyl, EIPA; 5-(N-ethyl-N-isopropyl)-amiloride, GFP; green fluorescent protein, HMA; hexamethylene amiloride, I-V; current-voltage relationship, IC_{50}; half maximal inhibitory concentration, MEM; Modified Eagle's Medium, MES; 4-morpholineethanesulfonic acid, NMDG; N-Methyl-D-glucamine, RMSD; root mean square deviation, SARS-CoV; SARS coronavirus, TEVC; two electrode voltage clamp, WT; wild type

Molecular Pharmacology Fast Forward. Published on May 18, 2016 as DOI: 10.1124/mol.115.102731
This article has not been copyedited and formatted. The final version may differ from this version.

Abstract

The increasing prevalence of influenza viruses with resistance to approved antivirals highlights the need for new anti-influenza therapeutics. Here we describe the functional properties of hexamethylene amiloride (HMA)-derived compounds that inhibit the wild-type and adamantane-resistant forms of the influenza A M2 ion channel. For example, 6-(azepan-1-yl)-*N*-carbamimidoylnicotinamide (**9**) inhibits amantadine-sensitive M2 currents with 3 to 6-fold greater potency than amantadine or HMA (IC_{50}s = 0.2 vs. 0.6 and 1.3 μM, respectively). Compound **9** competes with amantadine for M2 inhibition, and molecular docking simulations suggest that **9** binds at site(s) that overlap with amantadine binding. In addition, *tert*-butyl 4'-(carbamimidoylcarbamoyl)-2',3-dinitro-[1,1'-biphenyl]-4-carboxylate (**27**) acts both on adamantane-sensitive and a resistant M2 variant encoding a Serine to Asparagine 31 mutation (S31N) with improved efficacy over amantadine and HMA (IC_{50}s = 0.6 μM and 4.4 μM, respectively). While **9** inhibited *in vitro* replication of influenza virus encoding wild-type M2 (EC_{50} = 2.3 μM), both **27** and *tert*-butyl 4'-(carbamimidoylcarbamoyl)-2',3-dinitro-[1,1'-biphenyl]-4-carboxylate (**26**) preferentially inhibited viruses encoding M2(S31N) (respective EC_{50}s = 18.0 and 1.5 μM). This indicates that HMA derivatives can be designed to inhibit viruses with resistance to amantadine. Our study highlights the potential of HMA derivatives as inhibitors of drug-resistant influenza M2 ion channels.

Molecular Pharmacology Fast Forward. Published on May 18, 2016 as DOI: 10.1124/mol.115.102731
This article has not been copyedited and formatted. The final version may differ from this version.

Introduction

Viroporins are virally-encoded transmembrane proteins that facilitate conduction of ions or small molecules and are required for efficient viral replication (Nieva et al., 2012). Despite their small size (frequently < 100 amino acids), viroporins in many cases have evolved to function as highly regulated ion channels, which makes them attractive minimalist models of ion conductance and ion channel evolution (Pinto et al., 1992; Stouffer et al., 2008; Thiel et al., 2011; OuYang et al., 2013; OuYang & Chou, 2014). The M2 viroporin of influenza A is a 97 amino acid, type I transmembrane domain protein that forms a tetrameric ion channel that is proton-gated and proton-selective (Nieva et al., 2012). After viral entry into host cells, M2 conducts protons from acidic host cell endosomes to the virion interior to allow for uncoating and release of viral RNA. M2 on host cell endosomal membranes is also observed in some cases to conduct protons to elevate secretory vesicle pH, thereby delaying egress of nascent virion particles and preventing viral hemagglutinin from adopting a non-functional, low pH conformation (Sugrue et al., 1990; Alvarado-Facundo et al., 2015). The M2 ion channel of influenza B (B/M2) is a functional homolog of A/M2. It is 109 residues long and forms a homotetramer in the membrane like A/M2. Furthermore, B/M2 exhibits higher channel activity but shows a similar pH-dependence in terms of its proton conductance. There however exist major differences between the two channels; apart from the HXXXW sequence motif crucial for channel activity, the two proteins share nearly no sequence homology and unlike A/M2, the B/M2 proton conductance activity is entirely insensitive to amantadine and rimantadine. (Mould et al., 2003; Wang et al., 2009).

The compounds amantadine and rimantadine (Figure 1A) are potent inhibitors of A/M2 proton conductance and licensed influenza antivirals (Hay et al., 1985; Pinto et al., 1992; Chizhmakov et al., 1996). However, M2 sequence changes that render resistance to adamantanes are now so prevalent that these compounds are no longer recommended for use (Fiore et al., 2011). For example, over 90% of transmissible adamantane-resistant influenza strains encode an M2 serine to asparagine mutation at position 31 (S31N). This mutation disrupts adamantane interactions within the M2 pore without adversely affecting ion channel activity (Hay et al., 1986; Belshe et al., 1988; Pinto et al., 1992; Bright et al., 2005; Stouffer et al., 2008, Balannik et al., 2010). Thus, new small molecules that

inhibit adamantane-resistant M2 are desired for both improved understanding of the chemical space and mechanisms by which M2 activity can be modified in addition to development of new influenza antivirals.

To date, few compounds are reported to act on the S31N form of M2 from influenza A. Furthermore, several proposed M2 inhibitors that are derived from established M2 inhibitors and act on subsets of drug-resistant influenza viruses *in vitro* instead confer antiviral activity through alternative mechanisms (Jizhou Wang et al., 2013; Kolocouris et al., 2014), indicating that direct screening of M2 ion channel activity is necessary to identify *bona fide* M2(S31N) inhibitors. One of the most potent adamantane derivative for which detailed M2 current analysis is available, N-((5-(thiophen-2-yl)isoxazol-3-yl)methyl)adamantan-1-amine (**M2WJ352**; Figure 1A), inhibits M2(S31N) but not wild-type (WT) M2 proton currents as measured by two electrode voltage clamp (TEVC) electrophysiology, with an IC_{50} of 14 μM (Jun Wang et al., 2013).

A separate class of compounds that remains poorly explored for anti-M2 activity is the acylguanidines (Kleyman & Cragoe, 1988; Gazina & Petrou, 2012). Initially identified as potassium-sparing diuretics, acylguanidine-containing amilorides, and hexamethylene amiloride (**HMA**) in particular (Figure 1B), are inhibitors of multiple viroporins including those of HCV, HIV-1, and SARS-CoV (Kleyman & Cragoe, 1988; Ewart et al., 2002; Premkumar et al., 2004; Pervushin et al., 2009; Gazina & Petrou, 2012). HMA has also been reported to inhibit M2(WT) (IC_{50} = 1.1 μM by TEVC) but not M2(S31N), while a related compound N-(5-(1-methyl-1H-pyrazol-4-yl)naphthalene-2-carbonyl)guanidine (**BIT-225**; Figure 1B) inhibits currents from the viroporins of Hepatitis C and HIV-1 and shows promising activity in early clinical trials (Khoury et al., 2010; Luscombe et al., 2010; Gazina & Petrou, 2012). However, while additional acylguanidines including ethyl-isopropyl amiloride (**EIPA**) and (6-(1-methylpryazol-4-yl)-2-napthoyl)guanidinium (**BIT-314**; Figure 1B) are also reported to have antiviral activity against multiple viroporins and viruses, their effects on M2 currents are not yet reported (Ewart et al., 2009; Gazina & Petrou, 2012). Herein we describe an electrophysiology-driven approach to characterize the mechanism of and pharmacologically evaluate a series of acylguanidines and HMA-like derivatives on inhibition of wild-type and adamantane-resistant influenza M2 viroporins.

Materials and Methods

Chemistry. Detailed information for synthesis and characterization of compounds **1-33** can be found in Supplemental Material. **M2WJ352** was synthesized as described previously (Jun Wang et al., 2013). Amantadine hydrochloride, 5-(N,N-Hexamethylene)amiloride, 5-(N-Ethyl-N-isopropyl)amiloride, and 1-Benzoylguanidine were purchased from Sigma-Aldrich.

Electrophysiology. tsA-201 cells, a derivative of the HEK 293T cell line, or *ltk*- murine fibroblast (LM) cells were cultured in Modified Eagle's Medium plus 10% fetal calf serum, 100 U/mL penicillin, and 100 μg/mL streptomycin (MEM + medium). cDNA sequences encoding full-length M2 were derived from the A/Hong Kong/1073/99(H9N2) or B/Lee/1940 references sequence and contained an N-terminal FLAG-tag plus 3 (Gly) repeat linker. This tag was used to confirm M2(WT) expression on the cell surface of transfected cells by immunocytochemistry (Supplemental Figure 1). M2 sequences were cloned into the pcDNA3 plasmid and transiently co-transfected with a pcDNA3 plasmid encoding eGFP into tsA-201 cells using standard transfection protocols (Lipofectamine 2000, Life Technologies). 24-48 h after transfection, single GFP-positive cells were perfused continuously at 3-5 mL/min with external (bath) solution containing (in mM): 150 NMDG, 10 HEPES, 10 D-glucose, 2 $CaCl_2$, 1 $MgCl_2$ buffered at pH 7.4. For low external pH (pH_o 5.9 or 5.5) solution, HEPES was replaced by MES. Patch electrodes were pulled from thin-walled borosilicate glass (World Precision Instruments) and fire-polished before filling with standard pipette solution containing (in mM): 140 NMDG, 10 EGTA, 10 HEPES, and 1 $MgCl_2$ buffered at pH 7.2, or pH 6.0 (10 mM MES). M2 currents were detected in > 90% of GFP positive cells assayed during the course of the study.

Voltage-clamp experiments were performed with an Axopatch 200B amplifier (Molecular Devices, CA) connected to a Digidata1322A 16-bit digitizer. Pipettes typically had a resistance of 3-5 MΩ. Data were acquired with pCLAMP9.2 software (Molecular Devices, CA) sampled at 10 kHz and low-pass filtered at 5 kHz. The standard voltage protocol consisted of holding a cell at -40 mV, followed by a 100-ms pulse to -80 mV, a 300-ms ramp to +40 mV, and a 200-ms step to 0 mV before stepping back to -40 mV repeated every 4 s at 20-22 °C.

Compound screening. Compounds were prepared in DMSO at 100 mM and diluted with external pH 5.5 solution to desired concentrations. To measure inhibition of M2 currents by compounds, cells were exposed repeatedly to pH_o 7.4 and pH_o 5.5 solutions until stable, pH-dependent inward currents were reproducibly observed. Cells were then treated with compounds at defined concentrations in pH_o 5.5 solution for ≥ 2 min. Data are presented as percent current inhibition at a given concentration of compound or concentration required for 50% inhibition (IC_{50}). All compounds were initially tested at 100 µM. Compounds that showed greater than 50% inhibition at 100 µM were further tested at lower concentrations to estimate the half maximal inhibitory concentration (IC_{50}). This was calculated from nonlinear regression fitting of percentage inhibition at minimum of three concentrations, and experiments were performed at least three times at each concentration.

Current-voltage relations. M2-transfected *ltk*- murine fibroblast (LM) cells were used 18-48 h post-transfection. Cells were voltage clamped using the whole-cell patch clamp configuration described above. To maximize internal pH (pH_i) control, high concentrations of pH buffer were used as impermeant ions: The patch pipette contained 90 mM N-methyl-D-glucamine (NMDG), 10 mM EGTA and 180 mM N-2-hydroxyethylpiperazine-N'-2-ethanesulphonic acid (HEPES). The bath contained a similar solution with 2 mM $CaCl_2$ replacing EGTA. The pH of all solutions was lowered to desired values by addition of 5 M aqueous HCl. The osmolality of both bath solutions (pH_o 7.4 and 5.6) as well as the patch pipette solution were precisely adjusted to 300 mOsmol/kg by addition of glucose and measured by an osmometer (OsmetteII™ - Precision Systems Inc, MA). Membrane current was recorded at 20-22 °C, digitized at 10 kHz. Current was measured using a modified voltage ramp protocol that extended the voltage range from -80 to +120 mV. pH_i was held constant at 7.2, while pH_o was changed by fast perfusion close to the cell, and washout was by slow perfusion. M2 current-voltage relations were determined by subtracting current at pH_o 7.4, obtained during the ramp phase of the voltage protocol, from the activated M2 currents at pH_o 5.6, or from current after exposure to compound **9** or amantadine at pH_o 5.6. Reversal potentials (E_{rev}) were estimated by linear interpolation of data points of the I-V relation on each side of zero current.

Molecular Docking. Blind docking was carried out using AutoDock4.2 software (Morris et al., 1998) using the default parameters, the Lamarckian genetic algorithm with local search, and 25 million

energy evaluations (Long evals) per run. 150 runs were performed for **9**, 120 runs for **26** and 100 for **27**. The solution NMR structure of M2 (A/Hong Kong/156/97; PDB 2LY0) (Jun Wang et al., 2013), with **M2WJ332** removed, was used as the receptor. Autodock4.2 allows for 32 flexible bonds to be modeled; two were used for compound **9**, six for compound **26** and seven for compound **27**. The remaining bonds were used to allow flexibility of the side chains of Val27, Ser31, and His37. The remaining residues of the channel were held rigid during the docking process. The grid box size in initial runs were 20.25 x 30 x 20.25 angstroms in the x, y and z dimensions, which covered Ser23 to Arg45 of the crystal structure, and was expanded to 17.62 x 45 x 18.75 angstroms in subsequent runs to include Asp21 to Lys49, both centered around the inner pore. Figures were generated using PyMOL with the PyMOL Autodock Plugin (Seeliger & De Groot, 2010).

Cytotoxicity. tsA-201 cells were assessed for cell viability using the MTT reagent kit (Life Technologies). Cells were plated in 96-well plates ($2.5 \cdot 10^4$ cells / well) and incubated for 24 h, followed by treatment with drug for 24 h. Cells were then incubated with MTT reagent for 4 h and treated with an equal volume of 10% SDS + 0.01 M HCl, Cell cultures were read by spectrophotometry at an absorbance wavelength of 570 nm (A_{570}). A_{570} background values from wells without cells were subtracted from the A_{570} cell culture values and normalized to the average A_{570} value of cell cultures in the absence of compounds. Data were obtained from at least 3 experiments and at least 5 concentrations.

Generation of amantadine-sensitive and resistant influenza viruses. Recombinant influenza A viruses were generated using the reverse genetic system based on the A/Puerto Rico/8/34 (PR8) strain (Neumann et al., 1999) provided by Dr. Y. Kawaoka (University of Wisconsin, Madison). The endogenous M2 sequence of PR8 encodes both a threonine at position 27 (T27) and asparagine at position 31 (N31) that render amantadine resistance. Amantadine-sensitive PR8 viruses were therefore generated by mutating T27 and N31 to valine (V27) and serine (S31), respectively. Amantadine-resistant M2 encoding V27 and N31 was also generated. Nucleotide substitutions were introduced by modifying the sequence of pPol-PR8-MG-M (one of the 12 plasmids that make up the reverse genetics system) using two-step overlap extension PCR and cloning of subsequent DNA fragments into the pHH21 vector. A DNA fragment containing the S31 point mutation was generated

using the primers TSH289, TSH293, TSH294, and TSH292 (Supplemental Table 1) and pPol-PR8-HG-M (M2 T27 + N31) as the template. The PCR fragment and pHH21 vector were then treated with restriction endonuclease *Bsm*BI and ligated to generate pPol-PR8-HG-M-V27-N31 (M2 V27 + N31). A DNA fragment encoding V27 and S31 was generated using the same primers and pPol-PR8-HG-M-A27-S31 (M2 A27 + S31) as the template, which in turn was generated using primers TSH289, TSH290, TSH291, and TSH292 (Supplemental Table 1) and pPol-PR8-HG-M (M2 T27 + N31) as the template, resulting in generation of pPol-PR8-HG-M-V27-S31 (M2 V27 + S31). PCRs were performed using the Expand High Fidelity PCR System (Roche), and all constructs were confirmed by sequencing using primers TSH284 and TSH285 (Supplemental Table 1). Viruses were generated by transfecting one of the recombinant pPol-PR8-HG-M plasmids with the other 11 plasmids of the reverse genetics system to 293FT cells (Life Technologies). Cells were plated in a 6-well plate and transfected with the plasmid mixture (250 ng each) using TransIT LT-1 (Mirus). Culture supernatants were collected 48 h after transfection and passed through a 0.45 μm filter. After propagating virus in Madin-Darby canine kidney (MDCK) cells for 3-4 passages, virus stocks were stored at -80 ˚C.

Viral cytopathic assay. MDCK cells were cultured in DMEM (Life Technologies) plus 10% heat-inactivated fetal bovine serum (Hyclone), 100 U/mL penicillin, and 100 μg/mL streptomycin (Life Technologies) except during generation of virus stocks and plaque assays, when serum was removed from the media. Plaque reduction assays were carried out in triplicate as described (Song et al., 2005) with minor modifications. Briefly, approximately 100 plaque forming units of either PR8 recombinant with M2 V27 + S31 ($PR8_{M2(WT)}$) or one with M2 V27 + N31 ($PR8_{M2(S31N)}$) were mixed with different concentrations of the compounds, ranging from 100 μM to 1 μM, and inoculated on confluent MDCK monolayers in six-well plates. After a 1-hour adsorption at 37 °C, the inoculums were removed and cells were washed twice with phosphate-buffered saline (PBS). The cells were then overlaid with DMEM containing 1% Noble agar (Affymetrix), 10 mM HEPES buffer (Lonza), 0.00075% Difco™ Trypsin 250 (BD Biosciences), 100 U/mL penicillin, 100 μg/mL streptomycin, and each compound at test concentration. Following an incubation in 5% CO_2 at 37°C for three days, plaques were visualized and counted by staining the cells with 0.01% Neutral Red (Sigma-Aldrich). The concentration that reduces plaque number by 50% compared to the DMSO control (EC_{50}) was calculated by regression analysis of the dose–response curves.

Molecular Pharmacology Fast Forward. Published on May 18, 2016 as DOI: 10.1124/mol.115.102731
This article has not been copyedited and formatted. The final version may differ from this version.

Results

Detection of M2 currents by whole-cell patch-clamp electrophysiology. We initially investigated baseline M2 ion channel activity by co-transfecting tsA-201 cells with plasmids encoding GFP and M2(WT) (A/Hong Kong/1073/99(H9N2)) and recording pH-dependent ion currents in GFP-positive cells by whole-cell patch clamp electrophysiology (Figure 2; Chizhmakov et al., 1996; Kolocouris et al., 2014). Cells were held at a constant membrane potential of -40 mV, and currents were recorded every 4 s by applying 100 ms pulses to -80 mV. When M2-expressing (i.e., GFP-positive) cells were incubated in solution at pH_o 7.4 (designated by the horizontal black lines above each panel in Figure 2), minimal negative or inward current was observed (< 10 pA), which was normalized to 0.0 pA after all leak and initial current changes had settled down. In contrast, exposure to pH_o 5.9 – 5.5 (designated by the horizontal white rectangles above each panel) resulted in an initially large inward current that decayed ~50% during continued exposure to low pH_o. Return to pH_o 7.4 caused the steady inward current to deactivate. Subsequent, repeated exposures to extracellular acid solutions reversibly activated the relatively constant level of inward current (Figure 2A), consistent with previous observations (Kolocouris et al., 2014; Pinto et al., 1992). Currents were also detected in cells transfected with M2(WT) lacking the N-terminal FLAG epitope (data not shown) but not in cells transfected with only GFP control vector (Supplemental Figure 2).

Also consistent with previous reports (Pinto et al., 1992; Chizhmakov et al., 1996), extracellular administration of amantadine inhibited M2(WT) currents at acidic pH_o in a dose-dependent manner (Figure 2B), indicating that this protocol, which differs in cell-type, M2 strain, and pulse protocol from previous electrophysiology studies (Pinto et al., 1992; Chizhmakov et al., 1996), could be used to screen test agents for M2 current inhibition. No obvious differences were observed at pH_o 5.5 to 5.9 in efficacy or rate of M2 inhibition by amantadine and subsequent compounds (data not shown). For all compounds tested in this study, we obtained dose-response relationships if ≥ 50% inhibition of M2 current was observed at 100 μM. For amantadine, we determined an IC_{50} of 0.6 ± 0.2 μM (Table 1).

Using this protocol, we then screened four acylguanidine containing molecules (Figure 1B; Table 1). The most potent compound was **HMA**, which blocked M2(WT) currents with an IC_{50} of 1.3

Molecular Pharmacology Fast Forward. Published on May 18, 2016 as DOI: 10.1124/mol.115.102731
This article has not been copyedited and formatted. The final version may differ from this version.

± 0.3 μM (Figure 2C), followed by **EIPA**, which blocked M2(WT) currents with an IC_{50} of 52 ± 8 μM. In contrast, both **BIT-225** and **BIT-314** showed only modest activity against M2(WT) (30 ± 5% and 14 ± 2% inhibition of M2(WT) at 100 μM, respectively) and were not explored further.

Synthesis of a novel HMA derivative with improved activity against M2(WT). As HMA exhibited the most activity of the acylguanidines tested against M2(WT), we next asked which functional groups of HMA were responsible for its inhibitory activity. To test initially the role of central ring substitutions, we began by replacing the central pyrazine with a phenyl ring to generate compound **1**. Despite removal of the ring nitrogens, the exocyclic amino groups and the chloro atom, **1** exhibited improved activity against M2(WT) (IC_{50} = 0.4 ± 0.1 μM). In contrast, an analog of **1** with complete removal of the 7-membered azepane ring (**1-Benzoylguanidine**) had almost no activity (< 10% block; Table 1), indicating that a distal moiety is required. We did find that substitution of the azepane ring with cyclohexane was somewhat tolerated for anti-M2(WT) activity (e.g., **4**; IC_{50} = 5.0 ± 1.0 μM); however, this activity was sharply reduced when the cyclohexane was replaced with a more distally-polar morpholine ring (**6**; 33 ± 3% inhibition at 100 μM). Moreover, substitution with a pyrrolidine, benzene, or methoxybenzene was also less tolerated (IC_{50} = 50 ± 10 μM for **5**; 33% inhibition at 100 μM for **2** and **3**). Furthermore, the residual activity of **2** was abolished when the distal ring was shifted to the ortho or meta position of the central ring relative to acylguanidine (i.e., <10% block of M2(WT) by 100 μM of compounds **7**, or **8**), emphasizing the importance of ligand linearity, and consistent with our observations of limited anti-M2(WT) efficacy of non-linear molecules **BIT-225** and **BIT-314** (Table 1).

We next substituted a single phenyl carbon of **1** with nitrogen and synthesized compound **9**. Like **1**, compound **9** was also highly potent and inhibited M2(WT) current at pH_o 5.5 (Figure 3A), with an IC_{50} of 0.2 ± 0.1 μM (Table 1). In contrast, no inhibition of pH-dependent currents from the M2 ion channel of influenza B (B/Lee/1940) (Mould et al., 2003) was observed with up to 100 μM of **9** (Figure 3B)**,** demonstrating that the inhibitory activity of **9** is specific to M2 encoded by influenza A.

Further structure activity studies were performed using **9**. With respect to the central ring, replacing the pyridyl nitrogen with an exocyclic nitrogen in the form of a nitro group (**11**) also largely

Molecular Pharmacology Fast Forward. Published on May 18, 2016 as DOI: 10.1124/mol.115.102731
This article has not been copyedited and formatted. The final version may differ from this version.

retained activity against M2(WT) (IC_{50} = 1.8 ± 0.1 μM), but shifting the central pyridyl nitrogen to the ortho position relative to the acylguanidine moiety (**12**) substantially reduced activity (38 ± 7% inhibition at 100 μM). Similar to the compound **1** to **1-benzoylguanidine** transition, removal of the distal 7-membered azapane ring of **9** also eliminated activity (**10**). Moreover, removal of the guanidinium and/or carbonyl groups of the acylguanidine moiety (**13**, **14**, **15**) completely abolished or strongly reduced M2(WT) current inhibition at 100 μM (e.g., maximum 36 ± 3% inhibition for **15**; Table 1).

Compound **9** exhibited the most activity against M2(WT) currents, with almost an order of magnitude improved efficacy over the parent compound **HMA**. Moreover, and consistent with the docking model described below, molecule linearity combined with the presence of acylguanidine and distal ring moieties were necessary for M2(WT) activity, while some modifications to the central and distal rings were tolerated.

Effects of compound 9 on M2(WT) current-voltage relationships. We were interested to understand the voltage-dependence of **9** effects on pure M2 conductance in mammalian cells, and so carried out voltage clamp experiments in LM cells expressing M2(WT) protein. H^+ whole-cell currents were measured in the absence of other monovalent cations (Na^+ and K^+) using pipette and external media that contained only impermeant organic ions N-methyl D-glucamine ($NMDG^+$) and $HEPES^-$ or MES^-. Consistent with results obtained from tsA-201 cells, in LM cells transfected with M2(WT), a change in pH_o from 7.4 to 5.6 induced an inward current at -80 mV that was sensitive to both **9** (Figure 4A) and amantadine (Supplemental Figure 3). Current-voltage relationships obtained during the ramp phase of the protocol between -80 and +120 mV in pH_o 7.4, 5.6, and at pH_o 5.6 plus 100 μM **9** are shown in Figure 4B. It can be seen that all three relationships cross close to +80 mV. Subtraction of the relationship obtained at pH_o 7.4, which we assume contains little M2 current, from those at pH_o 5.6 places the reversal potential of the pH_o 5.6 relations on the zero current axis, and gives an E_{rev} of +80 mV (Figure 4C), which is close to the predicted reversal potential of +92 mV for a pure, M2-dependent H^+ current. Similarly, subtraction of the two relationships obtained at pH_o 5.6 gave the **9**-sensitive current (Figure 4D), which showed an E_{rev} of +85 mV, again close to that predicted for a pure H^+ current. The S.D of the data points around the best-fit line through the current-

voltage relations at their reversal potentials was ± 8 mV, indicating the overall error in estimating E_{rev}. These results suggest that lowered pH_o activates a relatively pure M2 H^+ current, and that **9** (Figure 4) and amantadine (Supplemental Figure 3) both directly inhibit M2 H^+ currents in these cells.

Molecular modelling of M2(WT) block. To gain insight into how **9**, **26** and **27** (described below) might bind and inhibit the M2 channel we performed molecular docking analyses (Huey et al., 2007; Morris et al., 1998; Seeliger & De Groot, 2010) with the M2 transmembrane domain tetramer (PDB entry 2LY0, the NMR structure of residues 19-49 of M2 of A/Chiba/5/71(H3N2) in dodecylphosphocholine micelles, computationally modified to include S31 when necessary; Jun Wang et al., 2013). In addition, we ran a compound that did not block in electrophysiological studies to observe the predictions made by the program. Due to constraints of the AutoDock 4 software that limit the number of flexible bonds in the ligand plus the receptor to 32 for accuracy (Trott & Olson, 2009), the M2 structure was largely held rigid during docking simulations with the exception of 3 flexible residues per tetramer subunit (Val27, Ser31 or Asn31 and His37). These residues were selected based on **9**'s interactions during a trial molecular docking simulation where M2(WT) was held entirely rigid, in addition to a visual scan for residues with side chains that were most obviously pointing into the inner vestibule and could provide steric hindrance if left rigid.

Using these parameters, we identified several binding sites for **9** (Figure 5A-5D). Many of the lowest energy binding conformations were in the turret (Figure 5A), and many did not actually block the channel, suggesting this might not be the block site. This is consistent with the fact that **9** does not block N31 (Table 2 and described below) and the two share identical sequence in the turret. Autodock also predicted in some conformations that the hydrophobic 7-membered azepane ring of **9** could pass through the constriction created by the valines at position 27 while the acyl guanidine portion maintained polar interactions with Ser22 and Asp24, creating an effective plug of the pore (Figure. 5B). Much of **9** block is readily reversible upon washout (Figure 5F), and this binding configuration might explain this reversibility since the majority of **9** remains outside the inner vestibule. The 20% block that is not reversible might then be a result of full entry of the drug into the inner vestibule (Figure 5C, 5D). Approximately 50% of predicted binding conformations were in the inner vestibule but all of these fell 1-2 kcal/mol higher in energy than the majority of turret binding conformations (-

13.61 to -11.85 kcal/mol). These could be with either the acyl guanidine pointing towards the valines (Figure 5C,D) or towards the histidines at position 37 (Supplemental Figure 6) with similar binding energies. However, if the initial trajectory of the passage involves a hydrophobic interaction between the 7-membered azepane ring and the valines, this would favour an inner vestibule orientation as shown in Figure 5C (shown in more detail in Figure 5D). In this conformation the 7-membered azepane ring is reaching down to interact with Histidine 37 from two subunits as well as the backbone of Leucine 38. In addition, the azepane ring and the central pyridyl ring make hydrophobic interactions with Gly34 and Ala30 respectively and the acyl guanidine interacts with valines that define the roof of the inner vestibule (Figure 5D).

Interestingly, mutations at multiple M2 residues predicted to interact with **9**, including Val27, Ala30, and Gly34, lead to adamantane resistance in vitro and/or in transmissible viruses (Hay et al., 1985, 1986; Belshe et al., 1988). Facets of the docking approach, such as use of an empirical hydration force field for the drug binding in the water-filled lumen and use of a micellar protein structure and homology model thereof, require a conservative interpretation confined to assessment of the steric fit of the drug in the pore. Nevertheless, taken together, these observations further support that **9** inhibits M2(WT), but potentially not M2(S31N), by a pore-blocking mechanism. That **9** does not block M2-N31, leads us to speculate that the extra bulk and hydrophilicity of the asparagine side chain hinders, or makes energetically unfavourable, the entry of the bulky hydrophobic 7-membered azepane ring of **9** into the inner vestibule of the mutant channel.

As **9** and amantadine are predicted to interact with many of the same M2 pore-lining residues, we next tested whether **9** and amantadine compete for M2(WT) inhibition (Figure 5E-H). Treatment of M2(WT)-expressing cells with 10 μM amantadine at pH_o 5.5 reduced pH-dependent currents by 63.5% (Figure 5E). However, following removal of amantadine from extracellular solution, little recovery of baseline M2(WT) current was observed after either at least 3.3 min at pH_o 5.5 (Figure 5E) or iterative treatment with pH_o 7.4 and pH_o 5.5 solutions (data not shown), consistent with previous observations that amantadine does not readily dissociate from blocked M2(WT) channels (Balannik et al., 2009, 2010). In contrast, while 10 μM of **9** reduced M2(WT)-dependent currents by 80.5% in Figure 5F, these currents recovered 57.1% within 3.3 min of removal of **9**, indicating reversible

inhibition and rapid recovery of M2(WT) currents. The different M2(WT) current recovery rates observed after removal of amantadine and **9** from pH_o 5.5 solution let us test which compound preferentially blocked M2 (WT) when applied in competition. As shown in Figure 5G, when 10 μM of **9** was administered at pH_o 5.5 to inhibit M2(WT) (90.5% inhibition in this example), no obvious further inhibition by 10 μM amantadine was observed. However, after removal of both compounds, M2(WT) current recovered by 58.0% after 5 min, consistent with a model where M2(WT) was inhibited primarily by **9** and amantadine was largely unable to dislodge it from the pore. These recovered M2(WT) currents were subsequently inhibited by 10 μM amantadine (data not shown), showing that removal of **9** from the pore allowed amantadine access. When 5 μM of **9** was used (Figure 5H), which resulted in 61% block, subsequent exposure to 10 μM amantadine caused a further reduction in current. This suggests that amantadine can access M2(WT) channels left unblocked by the lower concentration of **9.** Taken together, these experiments suggest that **9** and amantadine likely compete for the same or highly overlapping binding sites to inhibit M2(WT).

Activity of compound 9 against adamantane-resistant M2 sequence. To assess the inhibitory potential of **9** against mutant M2 viroporins, we examined inhibition of pH_o-dependent currents in tsA-201 cells expressing an A/Hong Kong/1073/99(H9N2) M2 sequence encoding S31N. pH-dependent currents from M2(S31N)-expressing cells were identical to those of cells expressing M2(WT) (Figure 6). Consistent with this mutation conferring adamantane resistance (Balannik et al., 2010; Williams et al., 2013), we observed that M2(S31N) was inhibited only 24 ± 1% by 100 μM amantadine and 10 ± 3% by 100 μM **HMA** in patch clamp experiments (Table 2). Similarly, sequential exposure to 10 and 100 μM of **9** at pH_o 5.5 had almost no activity on M2(S31N) as shown in Figure 6A and Table 2 (<10% inhibition).

Discovery of HMA derivatives with activity against M2(S31N). As M2(S31N) is the most prevalent adamantane-resistant mutation observed in transmissible influenza (Bright et al., 2005), we next asked if derivatives of **9** could inhibit M2(S31N). As S31N affects both the polarity and the size of the hydrophobic adamantane binding site (Wang et al., 2011; Williams et al., 2013), we hypothesized that modifications to the hydrophobic terminus of **9** incorporating more polar groups might improve M2(S31N) inhibition, perhaps by stabilizing proximal and/or distal interactions within

the M2(S31N) pore. We first measured whether M2(S31N) could be inhibited by compounds **6**, **16**, **18**, and **20**, which all contain polar substituents in the distal ring; however, these compounds had little or no activity at 100 μM (e.g., maximum 16 ± 4% inhibition for **16**; Table 2). Furthermore, 100 μM of **1** and **11** also had limited or no activity against M2(S31N) (e.g., maximum 10 ± 1% inhibition for **11**; Table 2), indicating that these central ring modifications, on their own, did not substantially improve activity against M2(S31N).

We then assessed the combined effects of a more polar, Boc-conjugated distal piperazine (i.e., **16**) with a polar nitro group on the central ring (i.e., **11**). Interestingly, this compound (**28**) inhibited M2(S31N) with slightly more than additive effects relative to **16** and **11** (32 ± 5% at 100μM; Table 2), indicating that both the nitro and terminal Boc group of the piperazine are needed for M2(S31N) inhibition. However, **28** did not inhibit M2(WT). This observation, combined with activity against M2(S31N) which is only slightly improved over amantadine, prompted us to continue exploring **28** derivatives with improved M2(S31N) and M2(WT) activities.

Following our identification of **28** as an early lead for M2(S31N) inhibition, we next found that substitution of the central ring nitro group with either a chlorine (**23)** or nitrile (**22)** reduced activity against M2(S31N) (<10% and 17 ± 8% at 100 μM respectively). Shifting of the nitro group to ortho position with regard to the acylguanidine moiety (**17)** also reduced activity (10 ± 5% at 100 μM). Activity against M2(S31N) was also eliminated by increasing the size of the second ring from piperazine (**28**) to homopiperazine (**21**), with inhibition less than 10% at 100 μM. Finally, compounds with different size carboxylates (**29** and **32**) and sulfonamide (**31**) did not exhibit potent activity against M2(S31N) (maximum 11 ± 8% at 100 μM). However, switching the Boc-conjugated piperazine (**28**) with a piperidine ring with a slightly more polar terminal group (**25**) resulted in a compound having the same level of efficacy. Replacing the heterocyclic ring with an aromatic ring (**26**) substantially improved activity against M2(S31N) (60 ± 7% at 100 μM; IC_{50} = 42 ± 5 μM; Figure 6B). Unlike **28**, compound **26** also had observable, albeit weak activity against M2(WT) (20 ± 5% inhibition at 100 μM; Figure 6C). Further substitution of a polar nitro group into the distal ring resulted in compound **27** which had even more activity against both M2(WT) and M2(S31N), with IC_{50}s of 0.6 μM and 4.4 μM, respectively.

Molecular Pharmacology Fast Forward. Published on May 18, 2016 as DOI: 10.1124/mol.115.102731
This article has not been copyedited and formatted. The final version may differ from this version.

In this way we identified multiple derivatives of **9** that inhibit M2(S31N) currents, with lead compounds **26** and **27** inhibiting M2(S31N) with greatly improved activity over **HMA** and amantadine while retaining submicromolar M2(WT) activity, in the case of **27**. As whole-cell patch clamp electrophysiology and TEVC are not directly comparable, we synthesized **M2WJ352** (Jun Wang et al., 2013), a potent adamantane derivative, and found its IC_{50} to be 44 µM (Table 2), some 10-fold weaker than **27**.

Molecular docking studies of M2(S31N) block by 26 and 27. When molecular docking studies were performed with **26** within the M2(S31N) pore, two confirmations with inverse orientations were again observed to interact with Val27, Ala30, Gly34, His37, and Leu38, along with Asn31 (Figure 6D-E). However, similar to **9**, the orientation of the acylguanidine differed by interacting with either one or more of the valines at position 27 (Figure 6D) or by interacting with the histidines of the proton sensor (Figure 6E). Both the guanidine amines and the oxygens of the nitro-substituted phenyl ring could form hydrogen bonds as shown in Figure 6D. Also in some conformations (still within 2.0 RMSD), the oxygens of the Boc terminal group contributed to hydrogen bonding with His37 or Asn31 (data not shown). Taken together, in comparison to **9**, the longer molecule of **26** with added bulk and polarity of both the nitro and Boc group may help stabilize interactions across more of the pore, thereby improving block against M2(S31N).

While **26** does not bind in the turret the variety of conformations observed for this compound was no less impressive than for **9** (Supplemental Figure 4). The compound could be found in an orientation with the acyl guanidine pointing towards the extracellular domain (Figure 6D and Supplemental Figure 4B) or cytoplasmically (Figure 6E, Supplemental Figure 4A) and at varying depths within the M2 pore. It is conceivable that since the lowest energy conformations are deeper in the pore (Figure 6D and E, Supplemental Figure 4A, B far left) that the other conformations are intermediate states of the compound as it progresses to a preferred binding site, though all of the conformations lead to block. **26** does not wash out upon solution change (data not shown) leading one to speculate that once at least the bulk of the drug is past the valine ring it is difficult to reverse the entry process.

Molecular Pharmacology Fast Forward. Published on May 18, 2016 as DOI: 10.1124/mol.115.102731
This article has not been copyedited and formatted. The final version may differ from this version.

Binding patterns for **27** were fairly similar whether there was a serine at position 31 or an asparagine. Averaged over many runs for each channel construct, Val27 was occupied ~67% of the time, Ala30 ~47%, Ser/Asn31 ~27%, and Gly34 ~16%. Again, compound **27** was found to bind the channel in "Boc up" or "Boc down" conformations. When Serine was present at position 31 the lower energy cluster was "Boc up" (Figure 7A(i), Supplemental Figure 5A) though 63% of the runs fell into one of the "Boc down" conformations. When asparagine was present, the lower energy clusters were "Boc down", as well 54% of runs fell into these two clusters (Figure 7A(iii, iv) Supplemental Figure 5B). The lowest energy conformation found in M2(N31) was almost a kcal/mol more than the lowest energy conformation found when serine was present, which is consistent with the electrophysiological data showing **27** to be almost 10 times more effective in blocking the WT channel (Tables 1 and 2).

The nitro-substituted phenyl rings tended to interact with the hydrophobic wall of the inner vestibule, Val27, Ala30, Ile33 and Gly34. The nitro groups on these phenyl rings interacted with serine or asparagine, and even histidine if the drug bound low enough in the pore, and occasionally hydrogen bonds were predicted (Figure 7A(iv)). When **27** bound residues in the turret, hydrogen bonds were much more common between the acyl guanidine hydrogens and the oxygens of Asp21, Ser22, Ser23 and Asp24. The Boc group made hydrophobic interactions, depending on the depth and orientation, with the carbons in the histidine side chains (Figure7A(ii,iv)), or with Ala30 and Val27 (Figure 7A (i,iii)). Given that the Boc group presents an hydrophobic terminus it is tempting to speculate that it is this end that would pass through the valine ring more readily and that the "Boc down" orientation might be favoured. Adding the bulkier, more hydrophilic asparagine just below the valine might make entry slightly less favourable.

Molecular docking of compound 14 onto M2. Compound 14 is one which failed to block M2(WT) at 100 μM (<10%, Table 1), and modeling frequently predicted that **14** would bind in the extracellular turret (Figure 7B) without blocking the channel with very low binding energy (-17.16 kcal/mol). Interactions were made with Asp21, Ser22, Ser23, Asp24, and sometimes with one of the valines, often with the amine hydrogens forming hydrogen bonds with the aspartic acid oxygens. It is likely possible that more than one molecule of **14** could in fact bind in the turret given the four-fold symmetry of the channel. Even in this situation, given that the compound is off the central axis of the

pore, there would be no block. Where a binding site was found in the internal vestibule, the lower energy conformations were almost 2 kcal/mol higher in energy than the turret site (-15.41 kcal/mol; not shown). Migration into the inner vestibule would require the high affinity turret site remain vacant to allow an additional molecule of **14** to pass. **14** is a smaller molecule than **9, 26** and **27**. It lacks the acyl guanidine of **9, 26** and **27** that provides bulk and length and the nitro groups bulking up the rings of **26** and **27**. It is likely for this reason that when **14** binds the channel it can fail to block the channel (Figure 7B).

***In vitro* cytotoxicity.** Compounds that inhibited > 50% of M2(WT) or > 30% of M2(S31N) currents at 100 μM were assessed for cytotoxicity. Using a standard MTT-based cell metabolic assay, no obvious effects were observed in tsA-201 cells incubated for 24 h with up to 100 μM amantadine, **M2WJ352**, or compound **9** (Table 1). In contrast, **HMA** inhibited growth of tsA-201 cells with a 50% cytotoxic concentration (CC_{50}) of 4.7 ± 0.3 μM. Thus, while **HMA** inhibits M2(S31) currents with comparable efficacy to the established inhibitor amantadine and **9**, it also has undesirable cellular toxicity consistent with previous observations (Balgi et al., 2013). Intermediate levels of cytotoxicity between **HMA** and **9** were observed for both inhibitors of M2(S31N) and other **9** derivatives (e.g., CC_{50} = 25 ± 5 μM for **26**, 55 ± 17 μM for **27**; Table 2).

***In vitro* activities against influenza viruses in a cytopathic assay.** As functional experiments were primarily performed to this point on heterologously-expressed M2 ion channels, we next determined the effects of select compounds on replication of influenza A virus *in vitro* using a viral cytopathic assay with MDCK cells (Table 3). Here, we used a previously-described reverse genetic system based on the A/Puerto Rico/8/34 (PR8) strain (Neumann et al., 1999) to generate PR8 strains encoding M2 with exclusively S31 ($PR8_{M2(WT)}$, containing both V27 and S31) or N31 ($PR8_{M2(S31N)}$ containing V27 and N31). As expected, amantadine exhibited antiviral activity against $PR8_{M2(WT)}$ but not $PR8_{M2(S31N)}$ in these assays (50% effective concentration (EC_{50}) < 1 μM for $PR8_{M2(WT)}$ vs. > 100 μM for $PR8_{M2(S31N)}$; Table 3). Compound **9** also inhibited $PR8_{M2(WT)}$ (EC_{50} = 2.3 ± 0.1 μM), consistent with results from patch clamp studies using M2(WT). Notably, **9** also exhibited ~10-fold weaker activity against $PR8_{M2(S31N)}$ (EC_{50} = 23 ± 5 μM). As **9** did not inhibit M2(S31N) currents at up to 100 μM, these observations suggest that compound **9** may have an additional antiviral mechanism in addition

to M2(WT) blockade. While off-target antiviral effects are frequently observed for multiple M2 inhibitors (Kolocouris et al., 2014), the disproportionate ability of **9** to inhibit $PR8_{M2(WT)}$ relative to $PR8_{M2(S31N)}$ replication is nevertheless consistent with its ability to exclusively inhibit M2(WT) in patch clamp studies and further suggests that the additional efficacy of compound **9** against $PR8_{M2(WT)}$ relative to $PR8_{M2(S31N)}$ is due to M2 blockade.

The previously described M2(S31N) inhibitor **M2WJ352** (Jun Wang et al., 2013) inhibited $PR8_{M2(S31N)}$ with an EC_{50} = 1.8 ± 0.7 μM, and with a ~19-fold reduced activity against $PR8_{M2(WT)}$ (EC_{50} = 34 ± 6 μM). As **M2WJ352** did not inhibit M2(WT) currents at up to 100 μM, these observations suggest that **M2WJ352**, like **9**, may have antiviral mechanisms in addition to M2(S31N) blockade. Similarly, $PR8_{M2(S31N)}$ replication was blocked by both **26** and **27** (EC_{50} vs. $PR8_{M2(S31N)}$ = 1.5 ± 0.1 μM and 18 ± 1 μM, respectively), but weaker activity against $PR8_{M2(WT)}$ was also observed (EC_{50} vs. $PR8_{M2(WT)}$ = 6.9 ± 1.6 μM and 40 ± 1 μM, respectively; Table 3). While the antiviral activity of **26** is consistent with electrophysiology studies, antiviral and electrophysiology profiles of **27** are discordant; thus the antiviral activity of **27** observed here is unlikely to be due primarily to M2 blockade. Finally, no obvious cellular toxicities in MDCK cells were observed for any tested compound with the exception of **26**, where clear cell death was observed only at higher concentrations (100 μM).

Molecular Pharmacology Fast Forward. Published on May 18, 2016 as DOI: 10.1124/mol.115.102731
This article has not been copyedited and formatted. The final version may differ from this version.

Discussion

Here we show that of four acylguanidine compounds previously reported to act against multiple viroporins and/or viruses (Gazina & Petrou, 2012), **HMA** had the most potent efficacy against influenza A M2(WT) currents, as measured by whole-cell patch-clamp electrophysiology. We then show that the **HMA** derivative **9** inhibits M2(WT) and has improved efficacy over amantadine and **HMA**, while inhibition of adamantane-resistant M2(S31N) can be achieved with other derivatives of this chemical class such as **26** and **27**. Using a combination of electrophysiological, molecular docking, and structure-activity relationship studies, we identify the transmembrane pore of the M2 tetramer as the likely interaction site of **9, 26** and **27**, which leads to M2 current block, in a region which overlaps the reported adamantane interaction site.

Mechanisms of block of M2(WT). The M2 protein can transfer protons selectively across membranes with a H^+ electrochemical gradient, a property consistent with its role in modifying virion and trans-Golgi pH during virus infection (Sugrue et al., 1990; Alvarado-Facundo et al., 2015). In LM cells expressing the M2 protein, with pH_i 7.2 and pH_o 5.6, the I-V plots were similar in conductance and shape across all transfected cells. The inhibitory effect of amantadine (Supplemental Figure 3) and **9** (Figure 4) brought about an identical compression of the current across all voltages, while the pH- and drug-dependent currents through M2 demonstrated a reversal potential close to the equilibrium potential for the transmembrane pH gradient at pH_o 5.6, suggesting that **9** and amantadine inhibited proton currents similarly in our experiments. Our initial molecular docking studies predicted that, in the lowest-energy state, **9** interacts within the M2(WT) pore in two different orientations (Figure 5, Supplemental Figure 6) in a manner reminiscent of the previously-described orientations of rimantadine and amantadine. While alternative models of **9**-M2(WT) interactions are clearly possible, our model is supported by the competition of **9** with amantadine for M2(WT) inhibition (Figure 5), similar effects on current-voltage relations, and the inability of **9** to inhibit currents from adamantane-resistant M2(S31N) (Figure 6A). Our structure-activity relationship study also identifies distinct moieties of **9** that are required to maintain anti-M2(WT) activity. For example, derivatives of **9** lacking portions of the acylguanidine group (e.g., **13**, **14**, and **15**) were less effective in inhibiting M2(WT), while removal of the azepane ring (compounds **10** and **1-benzoylguanidine**) or substitution

with smaller rings (compounds **2**, **3**, **4**, **5** and **6**) did not improve on the activity of **9 (Table 1)**. A linear molecule was also required for activity, as shifting of the distal ring to either ortho or meta position relative to the acylguanidine also eliminated activity (**7**, **8**). While some, but not all compounds with substitutions in the central pyridyl ring maintained activity against M2(WT) (e.g., **1** and **11**), **9** retained the most potent inhibition of M2(WT) of the novel compounds tested here. However, **9** was ineffective in blocking the adamantane-resistant M2(S31N) variant. We then envisioned that the polarity changes brought about by the S31N mutation would require a molecule with both a more distal polar end as well as a polar substitution on the central ring, and **28** bearing a Boc distal end and a nitro-substituted central ring appeared to bind and block the S31N mutant.

Mechanisms of block of M2(S31N). When compared to amantadine, **28** and **25** somewhat improved blockade of currents from adamantane-resistant M2(S31N) (32-33% inhibition at 100 μM). However, we did identify two other **HMA** derivatives, **26** and **27**, of which **26** showed improved potency against M2(S31N) with an IC_{50} of 42 ± 5 μM, and weak activity against M2(WT), while **27** exhibited a potent dual inhibitory effect against both M2(WT) as well as M2(S31N) with an IC_{50} of 4.4 ± 0.5 μM and 0.6 ± 0.1 respectively, as measured by whole-cell patch clamp (Table 1 and 2). Autodock predicts binding of **26** in S31 that would lead to block, and so the failure to see significant block in the electrophysiological experiments suggests that forces driving the drug into the pore are different between S31 and N31. The addition of the second set of oxygens on the second ring structure in **27** appears to overcome this. The overall orientation of **26** and **27** with M2(S31N) is, to a first approximation, similar to that of **9** with M2(WT). Both **26, 27** and **9** are predicted to enter their binding site in two orientations to interact variably with both the selectivity filter (Val27) and the proton sensor (His37) (Figure 5A-D and Figure 6D-E). The binding site for **26** and **27** is predicted to span from Val27 to His37 (Figure 6 and 7, Supplemental Figure 4 and 5) which also overlaps to a degree with the binding site previously reported by NMR for the less potent inhibitor **M2WJ332** (Jun Wang et al., 2013). Notably, the acylguanidine carbonyl of both **9**, **26** and **27** may contribute to an H-bond with Ser31 in M2(WT) (for **9**) or Val27 in M2(S31N) (for **26** and **27**), and removal of this acylguanidine carbonyl, as seen in compounds **14** and **15**, significantly reduced activity against M2(WT). Thus the ability of **26** and **27** to act on M2(S31N) appears to be driven primarily by the presence of the acylguanidine moiety, the second aromatic ring, an additional distal Boc group and

the central ring nitro that increase bulk and perhaps stabilize deeper interactions within the expanded M2(S31N) pore. The second aromatic ring of **26**, (in comparison to **28** with a piperazine ring) appears to play a critical role in further stabilizing hydrophobic interactions with the walls of the amphipathic pore.

Correlation of viral and electrophysiology assays. Interestingly, in viral assays (Table 3), both amantadine and **9** displayed significant activity against $PR8_{M2(WT)}$ but not $PR8_{M2(S31N)}$ virus, supporting that **9** targets this virus, at least in part, by inhibiting proton flux through M2. In contrast, both **M2WJ352** and **26** were more potent against $PR8_{M2(S31N)}$, further supporting their action against M2(S31N). We note that the limited ability of **9** to inhibit $PR8_{M2(S31N)}$, and **26** to inhibit $PR8_{M2(WT)}$ electrophysiologically, but significant antiviral activity against these isoforms, suggests that effects of the M2 block may be amplified *in vitro*, or indeed that these acylguanidine-based compounds may exhibit additional antiviral mechanisms, as previously suggested for adamantanes (Kolocouris et al., 2014). Notably, compounds **9**, **26**, and **27** also exhibited markedly reduced cytotoxicity compared to the parent compound **HMA** in MTT assays with tsA-201 cells, further suggesting that these compounds may be improved starting points for future antivirals compared with **HMA**.

In summary, we describe novel acylguanidine-containing inhibitors of M2 viroporins with binding mechanisms similar to adamantanes, with potent activity against wild-type and adamantane-resistant M2 ion channels and viruses. The novel **HMA** derivatives, including compounds **26** and **27** as dual inhibitors of both M2(WT) and M2(S31N), provide scaffolds that may aid in development of further non-adamantane compounds with improved inhibitory activity against drug-resistant forms of M2. These promising leads for additional medicinal chemistry optimization will also require further *in vivo* studies to assess their antiviral efficacy, stability, and pharmacokinetic parameters in animal disease models.

.

Molecular Pharmacology Fast Forward. Published on May 18, 2016 as DOI: 10.1124/mol.115.102731
This article has not been copyedited and formatted. The final version may differ from this version.

Acknowledgements

We thank Luping Yan, Hannah E. Boycott, Shunping Lin, Zhuren Wang, and Daniel Mendonca for superb technical assistance, Raymond Andersen and Luping Yan for assistance with mass spectrometry, and Zabrina Brumme and Mark Brockman for use of facilities and critical review of the manuscript.

Authorship Contributions

Participated in research design: Jalily, Tietjen, Miller, Eldstrom, Tai, Niikura, and Fedida.

Conducted experiments: Jalily, Tietjen, Miller, Eldstrom, Tai, Niikura, Chou, and Kwan.

Preformed data analysis: Jalily, Tietjen, Eldstrom, and Fedida.

Wrote or contributed to the writing of the manuscript: Tietjen, Jalily, Eldstrom, Tai, and Fedida.

References

Alvarado-Facundo E, Gao Y, Ribas-Aparicio RM, Jiménez-Alberto A, Weiss CD, and Wang W (2015) Influenza Virus M2 Protein Ion Channel Activity Helps To Maintain Pandemic 2009 H1N1 Virus Hemagglutinin Fusion Competence during Transport to the Cell Surface. *J Virol* **89**: 1975-1985.

Balannik V, Wang J, Ohigashi Y, Jing X, Magavern E, Lamb RA, DeGrado WF, and Pinto LH (2009) Design and pharmacological characterization of inhibitors of amantadine-resistant mutants of the M2 ion channel of influenza A virus. *Biochem* **48**:11872-11882.

Balannik V, Carnevale V, Fiorin G, Levine BG, Lamb RA, Klein ML, DeGrado WF, and Pinto LH (2010) Functional studies and modeling of pore-lining residue mutants of the influenza A virus M2 ion channel. *Biochem* **49**: 696-708.

Balgi AD, Wang J, Cheng DY, Ma C, Pfeifer TA, Shimizu Y, Anderson HJ, Pinto LH, Lamb RA, DeGrado WF, and Roberge M (2013) Inhibitors of the influenza A virus M2 proton channel discovered using a high-throughput yeast growth restoration assay. *PLoS ONE.* **8**, e55271.

Belshe RB, Smith MH, Hall CB, Betts R, and Hay AJ (1988) Genetic basis of resistance to rimantadine emerging during treatment of influenza virus infection. *J virol* **62**: 1508-1512.

Bright RA, Medina M, Xu X, Perez-Oronoz G, Wallis TR, Davis XM, Povinelli L, Cox NJ, and Klimov AI (2005) Incidence of adamantane resistance among influenza A (H3N2) viruses isolated worldwide from 1994 to 2005: a cause for concern. *Lancet* **366**: 1175-1181.

Chizhmakov IV, Geraghty FM, Ogden DC, Hayhurst A, Antoniou M, and Hay AJ (1996) Selective proton permeability and pH regulation of the influenza virus M2 channel expressed in mouse erythroleukaemia cells. *J Physiol* **494**: 329-336.

Ewart GD, Mills K, Cox GB, and Gage PW (2002) Amiloride derivatives block ion channel activity and enhancement of virus-like particle budding caused by HIV-1 protein Vpu. *Eur Biophys J* **31**: 26-35.

Ewart GD, Luscombe CA, and Miller M (2009) Hepatitis c antiviral compositions and methods. *US Patent* WO2009018609A1.

Fiore AE, Fry A, Shay D, Gubareva L, Bresee JS, and Uyeki TM (2011) Antiviral agents for the treatment and chemoprophylaxis of influenza: recommendations of the Advisory Committee on Immunization Practices. *MMWR Recomm Rep* **60**: 1-24.

Gazina EV and Petrou S (2012) Viral targets of acylguanidines. *Drug Discovery Today* **17**: 1039-1043.

Hay AJ, Wolstenholme AJ, Skehel JJ, and Smith MH (1985) The molecular basis of the specific anti-influenza action of amantadine. *EMBO J* **4**: 3021-4.

Hay AJ, Zambon MC, Wolstenholme AJ, Skehel JJ, and Smith MH (1986) Molecular basis of resistance of influenza A viruses to amantadine. *J Antimicrob Chemoth* **18**: 19-29.

Huey R, Morris GM, Olson AJ, and Goodsell DS (2007) A semiempirical free energy force field with charge-based desolvation. *J Comput Chem* **28**: 1145-1152.

Khoury G, Ewart G, Luscombe C, Miller M, and Wilkinson J (2010) Antiviral Efficacy of the Novel Compound BIT225 against HIV-1 Release from Human Macrophages. *Antimicrob Ag Chemoth* **54**: 835-845.

Kleyman TR and Cragoe EJ (1988) Amiloride and its analogs as tools in the study of ion transport. *J Membrane Biol* **105**: 1-21.

Kolocouris A, Tzitzoglaki C, Johnson FB, Zell R, Wright AK, Cross TA, Tietjen I, Fedida D, and Busath DD (2014) Aminoadamantanes with persistent in vitro efficacy against H1N1 (2009) influenza A. *J Med Chem* **57**: 4629-4639.

Luscombe CA, Huang Z, Murray MG, Miller M, Wilkinson J, and Ewart GD (2010) A novel Hepatitis C virus p7 ion channel inhibitor, BIT225, inhibits bovine viral diarrhea virus in vitro and shows synergism with recombinant interferon-α-2b and nucleoside analogues. *Antiviral Res* **86**: 144-153.

Morris GM, Goodsell DS, Halliday RS, Huey R, Hart WE, Belew RK, and Olson AJ (1998) Automated docking using a Lamarckian genetic algorithm and an empirical binding free energy function. *J Comput Chem* **19**: 1639-1662.

Mould JA, Paterson RG, Takeda M, Ohigashi Y, Venkataraman P, Lamb RA, and Pinto LH (2003) Influenza B virus BM2 protein has ion channel activity that conducts protons across membranes. *Dev Cell* **5**: 175-184.

Neumann G, Watanabe T, Ito H, Watanabe S, Goto H, Gao P, Hughes M, Perez DR, Donis R, Hoffmann E, Hobom G, and Kawaoka Y (1999) Generation of Influenza A Viruses Entirely from Cloned cDNAs. *Proc. Natl. Acad. Sci. U. S. A.* **96**, 9345-9350.

Nieva JL, Madan V, and Carrasco L (2012) Viroporins: structure and biological functions. *Nature Rev Microb* **10**: 563-574.

OuYang B, Xie S, Berardi MJ, Zhao X, Dev J, Yu W, Sun B, and Chou JJ (2013) Unusual architecture of the p7 channel from hepatitis C virus. *Nature* **498**: 521-5.

OuYang B, and Chou JJ (2014) The minimalist architectures of viroporins and their therapeutic implications. *Biochim Biophys Acta* **1838**: 1058-1067

Pervushin K, Tan E, Parthasarathy K, Lin X, Jiang FL, Yu D, Ardcharaporn V, Soong TW, Liu DX, and Torres J (2009) Structure and inhibition of the SARS coronavirus envelope protein ion channel. *PLoS Pathog* **5**: e1000511.

Pinto LH, Holsinger LJ, and Lamb RA (1992) Influenza virus M2 protein has ion channel activity. *Cell* **69**: 517-528.

Premkumar A, Wilson L, Ewart G, and Gage P (2004) Cation-selective ion channels formed by p7 of hepatitis C virus are blocked by hexamethylene amiloride. *FEBS Lett* **557**: 99-103.

Seeliger D and De Groot BL (2010) Ligand docking and binding site analysis with PyMOL and Autodock/Vina. *J Comput Aid Mol Des* **24**: 417-422.

Song JM, Lee KH, and Seong BL (2005) Antiviral Effect of Catechins in Green Tea on Influenza Virus. *Antiviral Res.* **68**, 66-74.

Stouffer AL, Acharya R, Salom D, Levine AS, Di Costanzo L, Soto CS, Tereshko V, Nanda V, Stayrook S, and DeGrado WF (2008) Structural basis for the function and inhibition of an influenza virus proton channel. *Nature* **451**, 596-9.

Sugrue RJ, Bahadur G, Zambon MC, Hall-Smith M, Douglas AR, and Hay AJ (1990) Specific structural alteration of the influenza haemagglutinin by amantadine. *EMBO J* **9**: 3469-3476.

Thiel G, Baumeister D, Schroeder I, Kast SM, Van Etten JL, and Moroni A (2011) Minimal art: or why small viral K+ channels are good tools for understanding basic structure and function relations. *Biochim Biophys Acta* **1808**: 580-588.

Trott O, and Olson AJ (2009) AutoDock Vina: Improving the speed and accuracy of docking with a new scoring function, efficient optimization, and multithreading. *J Comput Chem* **31**: 455-461.

Wang J, Pielak RM, McClintock MA and Chou JJ (2009) Solution structure and functional analysis of the influenza B proton channel. *Nat Struct Mol Biol* **16**: 1267-1271.

Wang J, Ma C, Fiorin G, Carnevale V, Wang T, Hu F, and DeGrado WF (2011) Molecular dynamics simulation directed rational design of inhibitors targeting drug-resistant mutants of influenza A virus M2. *J Am Chem Soc* **133**: 12834-12841.

Wang Jizhou, Ma C, Wang J, Jo H, Canturk B, Fiorin G, DeGrado WF (2013) Discovery of Novel Dual Inhibitors of the Wild-Type and the Most Prevalent Drug-Resistant Mutant, S31N, of the M2 Proton Channel from Influenza A Virus. *J Med Chem* **56**: 2804-2812.

Wang Jun, Wu Y, Ma C, Fiorin G, Wang J, Pinto LH, Lamb RA, Klein ML, and Degrado WF (2013) Structure and inhibition of the drug-resistant S31N mutant of the M2 ion channel of influenza A virus. *P Natl Acad Sci USA* **110**: 1315-1320.

Williams JK, Tietze D, Wang J, Wu Y, DeGrado WF, and Hong M (2013) Drug-induced conformational and dynamical changes of the S31N mutant of the influenza M2 proton channel investigated by solid-state NMR. *J Am Chem Soc* **135**: 9885–97.

Molecular Pharmacology Fast Forward. Published on May 18, 2016 as DOI: 10.1124/mol.115.102731
This article has not been copyedited and formatted. The final version may differ from this version.

Footnotes

This work was funded by a Canadian Institutes of Health Research Industry-Partnered Collaborative Research Operating Grant [IPR-124291] which was co-funded by Cardiome Pharma Corp., Vancouver, Canada. We also wish to acknowledge the support from Grand Challenges Canada [0487-01-10]. Grand Challenges Canada is funded by the Government of Canada and is dedicated to supporting Bold Ideas with Big Impact in global health

Molecular Pharmacology Fast Forward. Published on May 18, 2016 as DOI: 10.1124/mol.115.102731
This article has not been copyedited and formatted. The final version may differ from this version.

Figure Legends

Figure 1. Examples of reported M2 inhibitors. **A**, Adamantane inhibitors; Amantadine, Rimantadine, and N-((5-(thiophen-2-yl)isoxazol-3-yl)methyl)adamantan-1-amine **(M2WJ352)** (Wang et al., 2013). **B**, Acylguanidines; hexamethylene amiloride (**HMA**) (Gazina & Petrou, 2012), N-(5-(1-methyl-1H-pyrazol-4-yl)naphthalene-2-carbonyl)guanidine (**BIT-225**) (Khoury et al., 2010; Luscombe et al., 2010), ethyl-isopropyl amiloride (**EIPA**), and (6-(1-methylpryazol-4-yl)-2-napthoyl)guanidinium (**BIT-314**).

Figure 2. Representative diary plots of pH-dependent currents detected at -80 mV from single tsA-201 cells transiently co-expressing GFP and M2(WT) (A/Hong Kong/1073/99 (H9N2)). **A,** Representative M2 current. Dots denote currents recorded at -80 mV every 4 s. In the presence of pH_o 7.4 solution (denoted by thin black lines above the traces), minimal inward or negative current is observed. When pH_o 5.9 solution is applied (denoted by white bars above the traces), an initially large inward current is observed, which eventually normalizes and is reversible with repeated pulses of pH_o 7.4 or pH_o 5.9 solution. H9N2 M2(WT) currents are dose-dependently inhibited by amantadine (**B**), and HMA (**C**). Data from each panel are representative of at least 3 independent experiments.

Figure 3. Effects of increasing concentrations of compound **9** on currents from tsA-201 cells expressing **A**, M2 (H9N2)(WT). **B**, B/M2. As for Fig.2, these are diary plots of currents measured at -80 mV every 4 s.

Figure 4. Current-voltage relations of H^+-activated current and block by **9: A,** Diary plot of M2 (WT) current against protocol pulse number. Cells were pulsed every 6 s from a holding potential of -40 mV, first to -80 mV for 200 ms and then ramped for 600 ms to +120 mV, a 400 ms repolarization to 0 mV, and then back to -40 mV. A current reading was taken at -80 mV and plotted against pulse number. Cells were exposed to pH_o 7.4 solution twice as denoted by the thin black bar above the graph, to pH_o 5.6 during the periods denoted by the thick bars, and also to pH_o 5.6 + 100 μM compound **9 (**grey thick bar**)**. Current voltage relations obtained under the three conditions at the times indicated in (A) by the symbols are plotted in panel **B**. All three relationships show mild inward rectification, but cross at ~+80 mV. **C**, Current activated at pH_o 5.6, before and in the presence of 100 μM compound **9**, obtained by subtracting current at pH_o 7.4. **D**, compound **9**-sensitive current only, obtained by subtracting relationships in pH_o 5.6, before and after compound **9** exposure, E_{rev}=+85 mV.

Figure 5. Mechanism of inhibition by **9. A**,**B**,**C** Models of **9** interacting with the transmembrane pore of M2(WT) (PDB entry 2LY0; residues 19-49 of M2 of A/Chiba/5/71(H3N2)) (Wang et al., 2013). Illustrated as a stepwise process, (**A**) the compound first encounters the turret but does not usually block at this stage; (**B**) the 7-membered azepane ring passes through the narrow ring created by Valines at position 27, (**C** and **D**) and then the rest of the compound follows to bind within the inner vestibule. Predicted binding energies were -15.06 kcal/mol (**A**),-12.54 kcal/mol (**B**) -14.61 kcal/mol (**C** and **D**). (**D**) Interacting residues of M2 are shown in stick format while the rest of M2 is in line format. The –A or –D after each numbered residue in this and later figures denotes which of the four tetramer subunit from which the amino acid originates. Only interacting residues are labeled. Hydrogens are hidden for clarity. Figure was created using AutoDock and PyMOL with the PyMOL Autodock Plugin (Seeliger & De Groot, 2010). **E-H**, Plots of normalized H9N2 M2(WT) currents in cells exposed to extracellular pH 5.5 solution with addition of either amantadine (**E**), **9** (**F**), amantadine added in presence of **9 (G)**, or amantadine followed by and in the presence of **9** (**H**). Data in panels **E-H** are representative of 4 independent experiments.

Figure 6. M2 current inhibition by HMA derivatives. **A. 9** does not inhibit H9N2 M2(N31) but (**B**) compound **26** inhibits H9N2 M2(S31N) with an IC_{50} = 42±5 μM, and (**C**) H9N2 M2(S31) by 20% at

50 µM. **D-E**. Models of **26** interacting with the transmembrane pore of M2(S31N) (PDB entry 2LY0; residues 19-49 of M2 of A/Chiba/5/71(H3N2)) (Wang et al., 2013). Lowest energy conformations of **26** in "up" **(D)** and "down" **(E)** configurations docked into M2. The predicted binding energies were -14.55 kcal/mol **(D)** and -14.35 kcal/mol **(E)**. **26** and interacting residues of M2 are shown in stick format while the rest of M2 is in line format. Only interacting residues are labeled. Hydrogens are hidden for clarity. Predicted H-bonds with a bond distance of 3.2 angstroms or less are shown by black dotted lines.

Figure 7. A. Mechanism of inhibition by 27. **A.(i,ii)** Models of **27** interacting with the transmembrane pore of M2(WT) (PDB entry 2LY0; residues 19-49 of M2 of A/Chiba/5/71(H3N2)) (Wang et al., 2013). **A.(iii,iv)** Models of **27** interacting with M2(N31) Predicted binding energies were -15.10 kcal/mol (**i**),-14.91 kcal/mol (**ii**) -14.31 kcal/mol (**iii**) and -13.44 kcal/mol (**iv**). Interacting residues of M2 are shown in stick format while the rest of M2 is in line format. Figure representation as for Figures 5 and 6. **B.** AutoDock predicted binding of **14** to M2(WT). **B(i,ii)**. Compound **14** sits in the extracellular turret region of the channel but does not block the channel (lowest binding energy=-17.16 kcal/mol). (**i**) **14** (carbons coloured pink) and M2 (carbons coloured green) are shown as atomic spheres. The channel is being viewed from the extracellular domain through to the cytoplasmic domain. The narrowest points in the pore are the valines at position 27 (indicated by arrows for 2 subunits) and the histidines at position 37 that create the narrowing in the distance. **B(ii)**. Same conformation as in **i**. this time residues of the channel interacting with **14** are represented by mesh spheres and the rest of the channel is in stick form. Labeled residues are those that are flexible (Val27, Asn31 and His37) for orientation purposes as well as those interacting with **14**.

Table 1. Properties of Amantadine, HMA, and acylguanidine derivatives on H9N2 M2(WT). SAR investigation of analogues with activity against the S31 M2(WT). Column 6 of table shows cell survival determined from MTT assay.

	R	Compound	A/M2 WT (mean ± SD)		Cell Survival MTT assay
			Inhibition by 100 µM (%)	IC_{50} (µM)	Estimated CC_{50} (µM) (N≥3)
Amantadine			>99	0.6 ± 0.2	>100
HMA			>99	1.3 ± 0.3	4.7 ± 0.3
BIT-225			30 ± 5	ND	
EIPA			63 ± 2	52 ± 8	
BIT314			14 ± 2	ND	
M2WJ352			<10	ND	>100
		**1**	>99	0.4 ± 0.1	4.9 ± 1.2
		**1-Benzoylguanidine**	<10	ND	
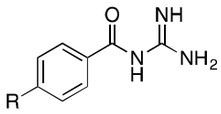		**2**	33 ± 8	ND	
		**3**	33 ± 5	ND	
		**4**	>99	5.0 ± 1	5.9 ± 1.9
		**5**	56 ± 2	50 ± 10	24 ± 8
		**6**	33 ± 3	ND	
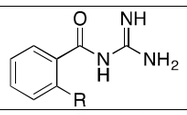		**7**	<10	ND	
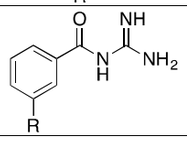	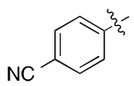	**8**	<10	ND	
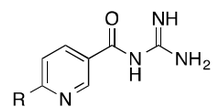		**9**	**>99**	**0.2 ± 0.1**	**>100**
		**10**	<10	ND	
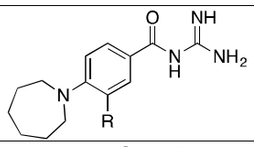		**11**	>99	1.8 ± 0.1	55 ± 11
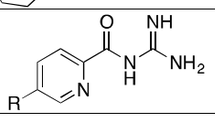		**12**	38 ± 7	ND	
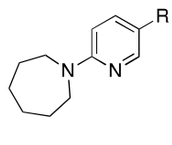		**13**	16 ± 4	ND	
		**14**	<10	ND	
	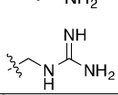	**15**	36 ± 3	ND	
26*			20 ± 5	ND	25 ± 5
27*			**>99**	**0.6 ± 0.1**	**55 ± 17**
28*			<10	ND	>100

ND., not determined. R., substitution. *Structures are shown in Table No. 2

Molecular Pharmacology Fast Forward. Published on May 18, 2016 as DOI: 10.1124/mol.115.102731
This article has not been copyedited and formatted. The final version may differ from this version.

Table 2. Properties of acylguanidine derivatives on H9N2 M2(S31N). SAR investigation of analogues with activity against the N31 mutant. In column 5, where an IC_{50} has been measured it is explicitly stated. Last column of table shows cell survival determined from MTT assay.

	R	X	Compound	A/M2 S31N (mean ± SD) Inhibition by 100 uM (%)	Cell Survival MTT assay Estimated CC_{50} (µM) (N≥3)
Amantadine				24 ± 1	>100
HMA				10 ± 3	4.7 ± 0.3
M2WJ352				75 ± 5 IC_{50} = 44 ± 4	>100
9*				<10	>100
11*				10 ± 8	55 ± 11
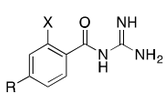	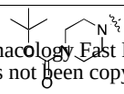		**16**	1.6 ± 1.1	
	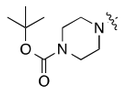		**17**	10 ± 5	
			**5**	<10	
			**6**	<10	
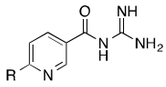		-	**18**	<10	
	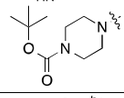	-	**19**	<10	
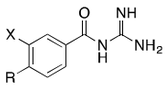			**20**	<10	
	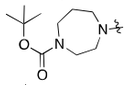		**21**	<10	
	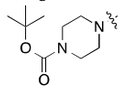		**22**	17 ± 8	
	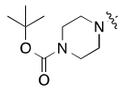		**23**	<10	
	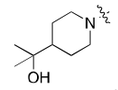		**24**	<10	
	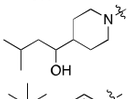		**25**	33 ± 15	58 ± 11
	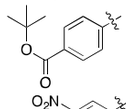		**26**	**60 ± 7** **IC_{50} = 42± 5**	**25 ± 5**
	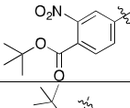		**27**	**>99** **IC_{50} = 4.4 ± 0.5**	**55 ± 17**
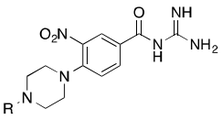		-	**28**	32 ± 5	>100
	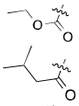	-	**29**	11 ± 0	
		-	**30**	<10	
		-	**31**	<10	
		-	**32**	<10	
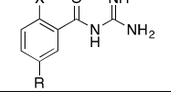	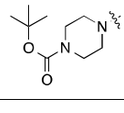		**33**	<10	

R., substitution. * Structures are shown in Table No. 1

Molecular Pharmacology Fast Forward. Published on May 18, 2016 as DOI: 10.1124/mol.115.102731
This article has not been copyedited and formatted. The final version may differ from this version.

Table 3. Antiviral activities from viral cytopathic assay of selected derivatives of acylguanidine against S31 and N31 forms of the A/PR/8/1934(H1N1) V27 influenza virus.

Compound	Viral Cytopathic Assay	
	Estimated EC_{50} (μM)	
	A/PR/8/1934(H1N1) V27	
	S31	N31
Amantadine	<1	>100
M2WJ352	34 ± 6	1.8 ± 0.7
9	2.3 ± 0.1	23 ± 5
26	6.9 ± 1.6	1.5 ± 0.1
27	40 ± 1	18 ± 1

Molecular Pharmacology Fast Forward. Published on May 18, 2016 as DOI: 10.1124/mol.115.102731
This article has not been copyedited and formatted. The final version may differ from this version.

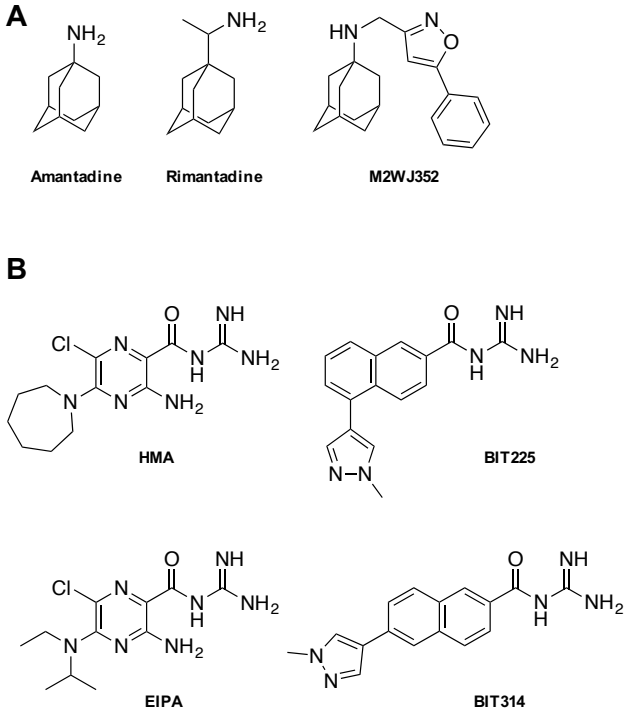
A
NH2
NH2
HN
N
O
Amantadine
Rimantadine
M2WJ352
B
Cl
N
O
NH
N
H
NH2
N
N
NH2
HMA
N–N
BIT225
EIPA
BIT314

Figure 1

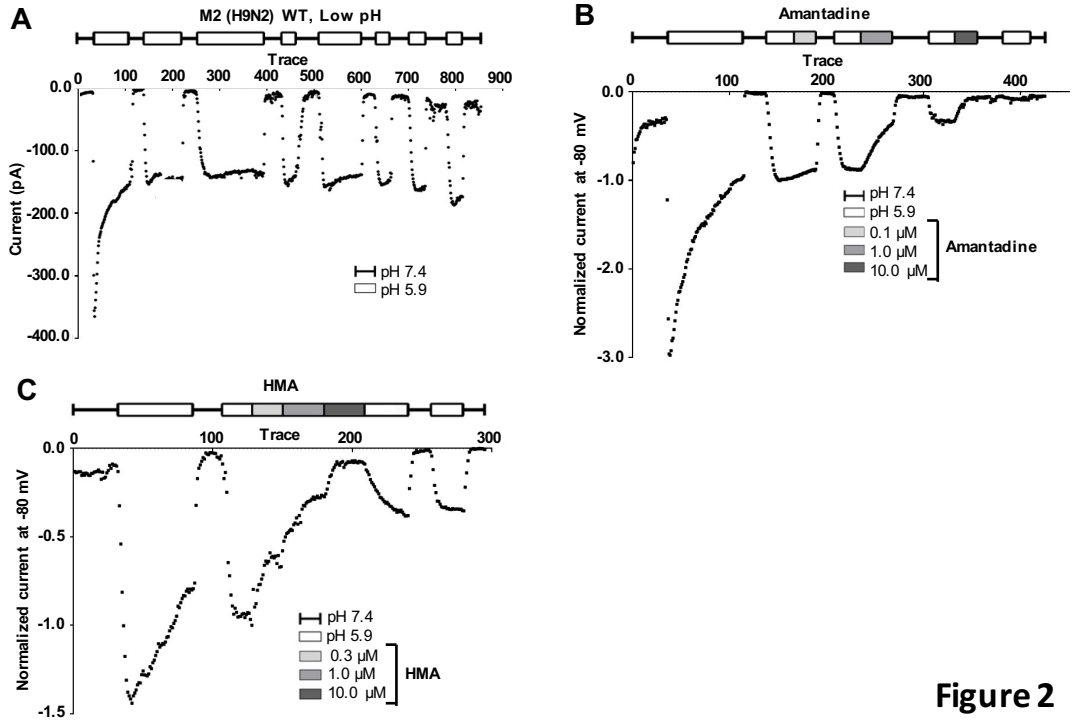
A
M2 (H9N2) WT, Low pH
Trace
0
100
200
300
400
500
600
700
800
900
0.0
-100.0
-200.0
-300.0
-400.0
Current (pA)
pH 7.4
pH 5.9
B
Amantadine
Trace
0
100
200
300
400
0.0
-1.0
-2.0
-3.0
Normalized current at -80 mV
pH 7.4
pH 5.9
0.1 μM
1.0 μM
10.0 μM
Amantadine
C
HMA
Trace
0
100
200
300
0.0
-0.5
-1.0
-1.5
Normalized current at -80 mV
pH 7.4
pH 5.9
0.3 μM
1.0 μM
10.0 μM
HMA

Figure 2

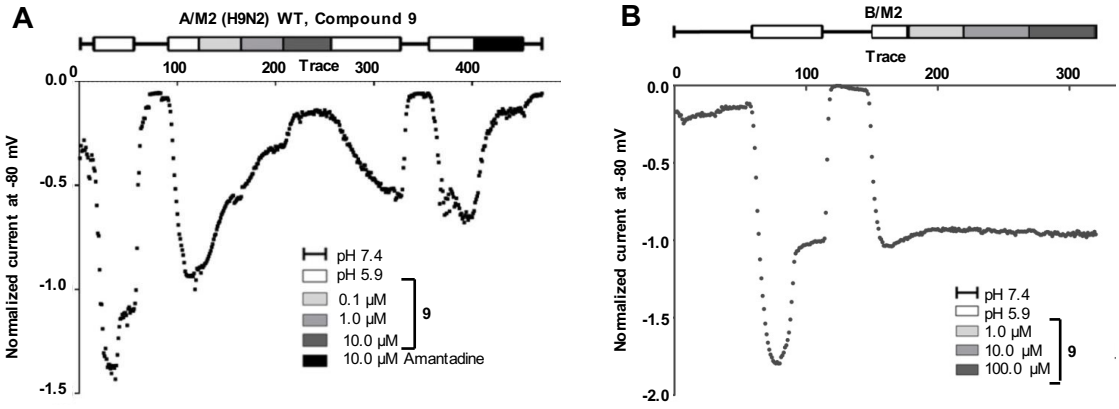
A
A/M2 (H9N2) WT, Compound 9
Trace
0
100
200
300
400
0.0
-0.5
-1.0
-1.5
Normalized current at -80 mV
pH 7.4
pH 5.9
0.1 µM
1.0 µM
10.0 µM
10.0 µM Amantadine
9
B
B/M2
Trace
0
100
200
300
0.0
-0.5
-1.0
-1.5
-2.0
Normalized current at -80 mV
pH 7.4
pH 5.9
1.0 µM
10.0 µM
100.0 µM
9

Figure 3

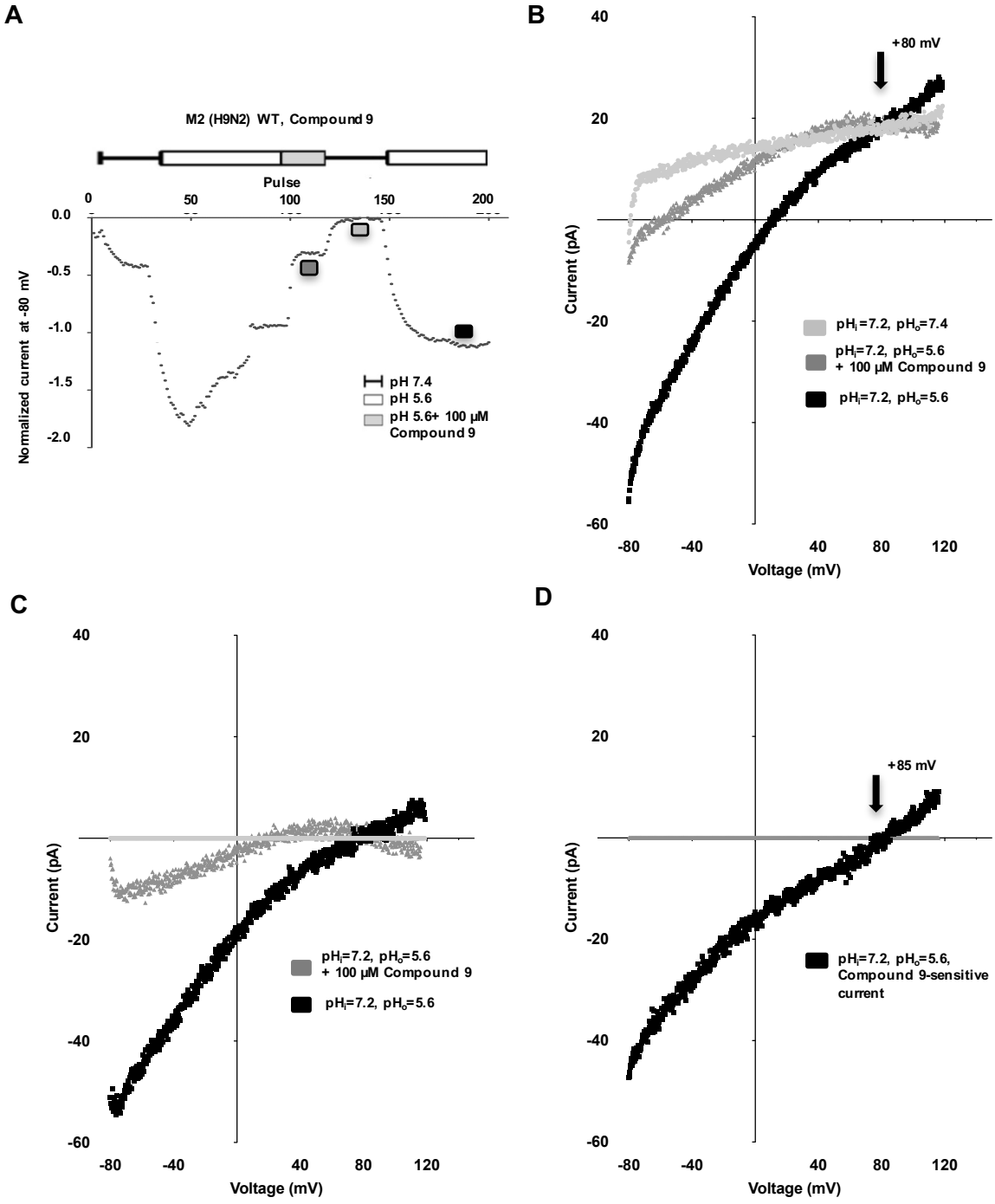
A
M2 (H9N2) WT, Compound 9
Pulse
0
50
100
150
200
0.0
-0.5
-1.0
-1.5
-2.0
Normalized current at -80 mV
pH 7.4
pH 5.6
pH 5.6+ 100 µM Compound 9
B
+80 mV
40
20
-20
-40
-60
Current (pA)
-80
-40
40
80
120
Voltage (mV)
pH$_i$=7.2, pH$_o$=7.4
pH$_i$=7.2, pH$_o$=5.6 + 100 µM Compound 9
pH$_i$=7.2, pH$_o$=5.6
C
40
20
-20
-40
-60
Current (pA)
-80
-40
40
80
120
Voltage (mV)
pH$_i$=7.2, pH$_o$=5.6 + 100 µM Compound 9
pH$_i$=7.2, pH$_o$=5.6
D
40
20
-20
-40
-60
Current (pA)
+85 mV
-80
-40
40
80
120
Voltage (mV)
pH$_i$=7.2, pH$_o$=5.6, Compound 9-sensitive current

Figure 4

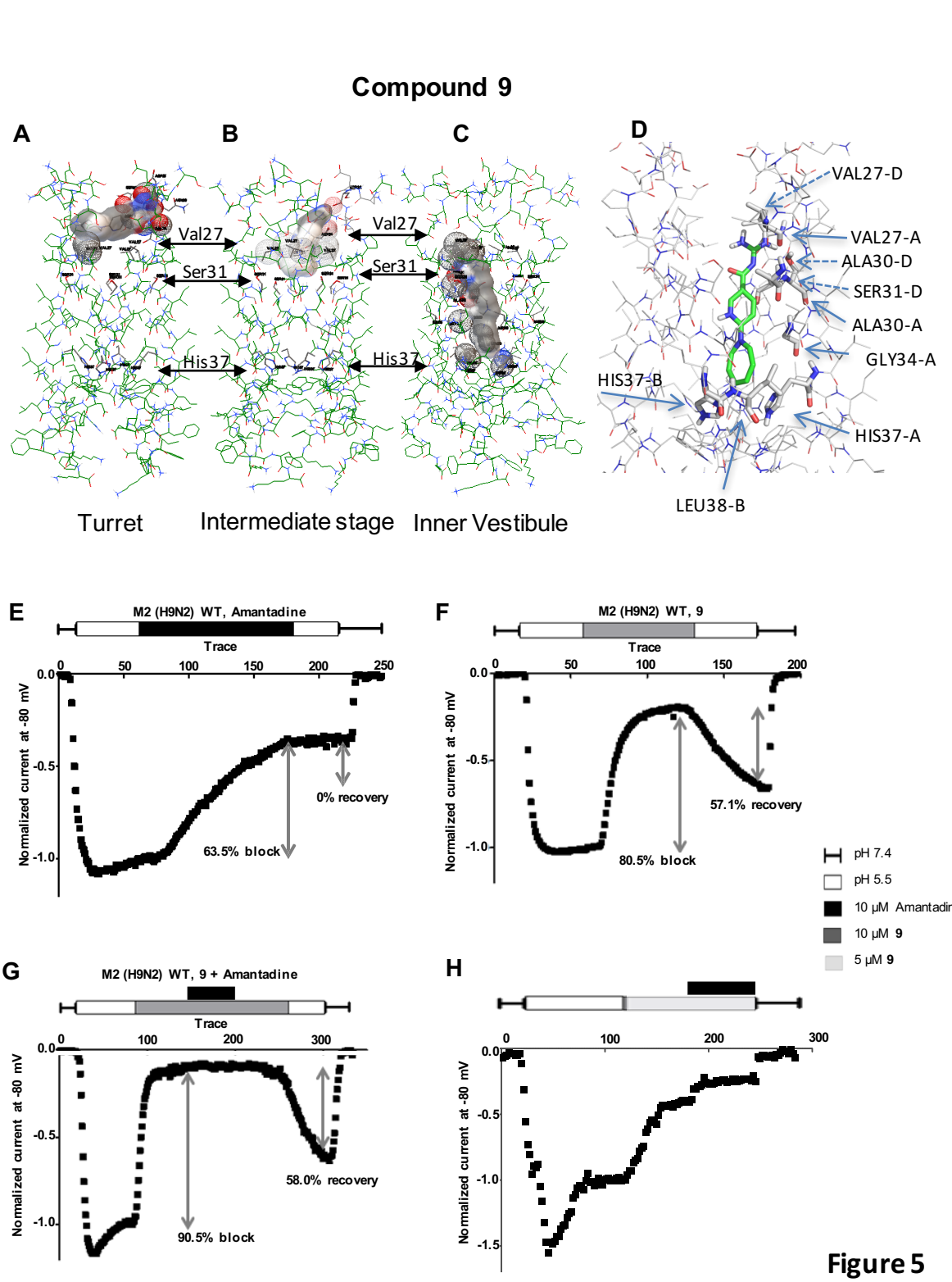
Compound 9
A
B
C
D
Val27
Ser31
His37
Val27
Ser31
His37
VAL27-D
VAL27-A
ALA30-D
SER31-D
ALA30-A
GLY34-A
HIS37-B
HIS37-A
LEU38-B
Turret
Intermediate stage
Inner Vestibule
E
M2 (H9N2) WT, Amantadine
Trace
Normalized current at -80 mV
63.5% block
0% recovery
F
M2 (H9N2) WT, 9
Trace
Normalized current at -80 mV
80.5% block
57.1% recovery
pH 7.4
pH 5.5
10 μM Amantadine
10 μM 9
5 μM 9
G
M2 (H9N2) WT, 9 + Amantadine
Trace
Normalized current at -80 mV
90.5% block
58.0% recovery
H
Normalized current at -80 mV

Figure 5

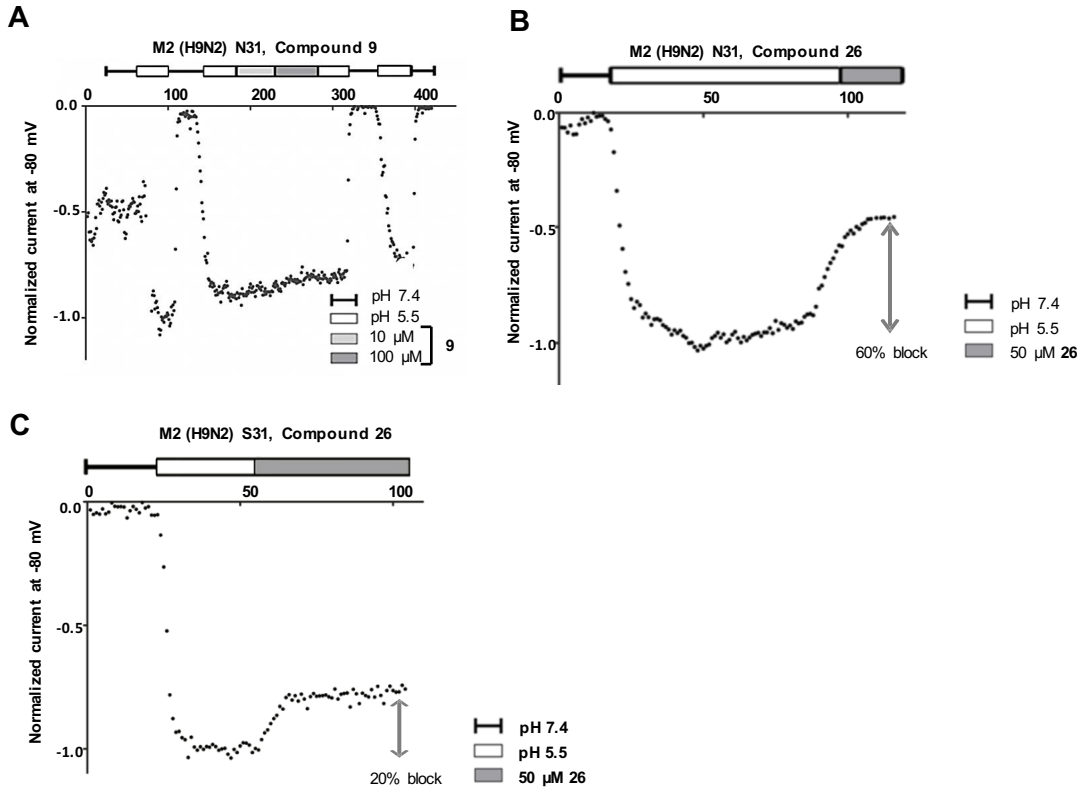

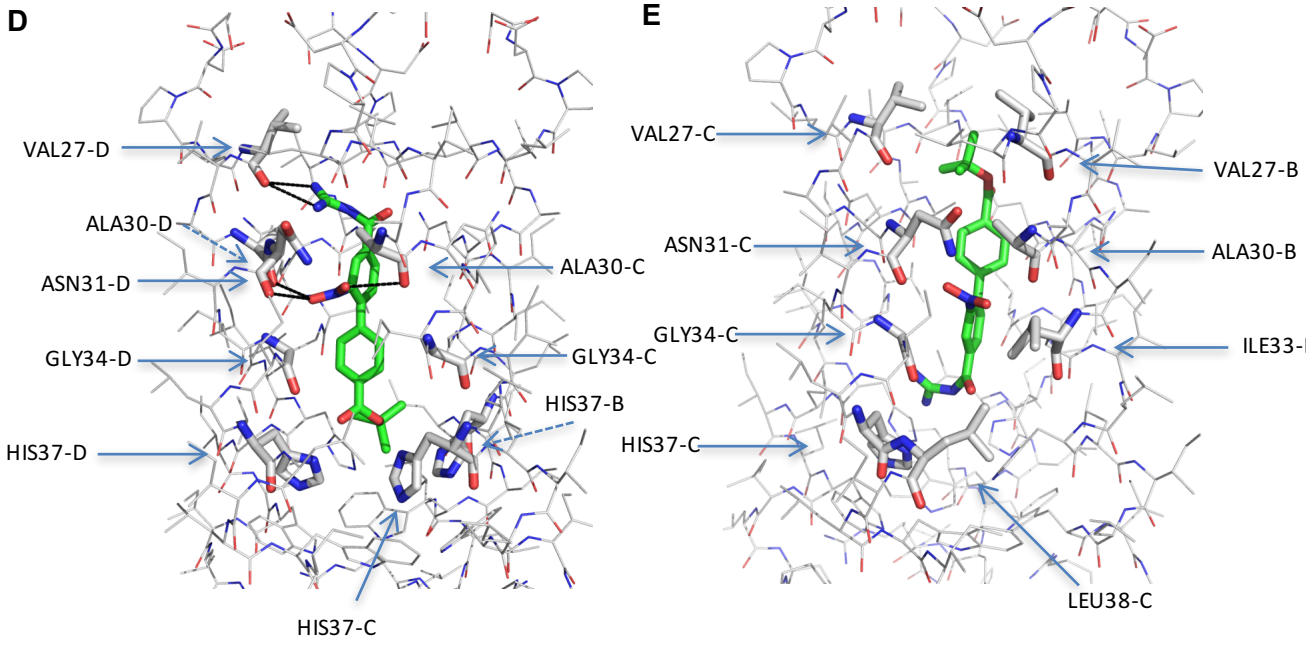

Compound 26

Figure 6

A

Compound 27

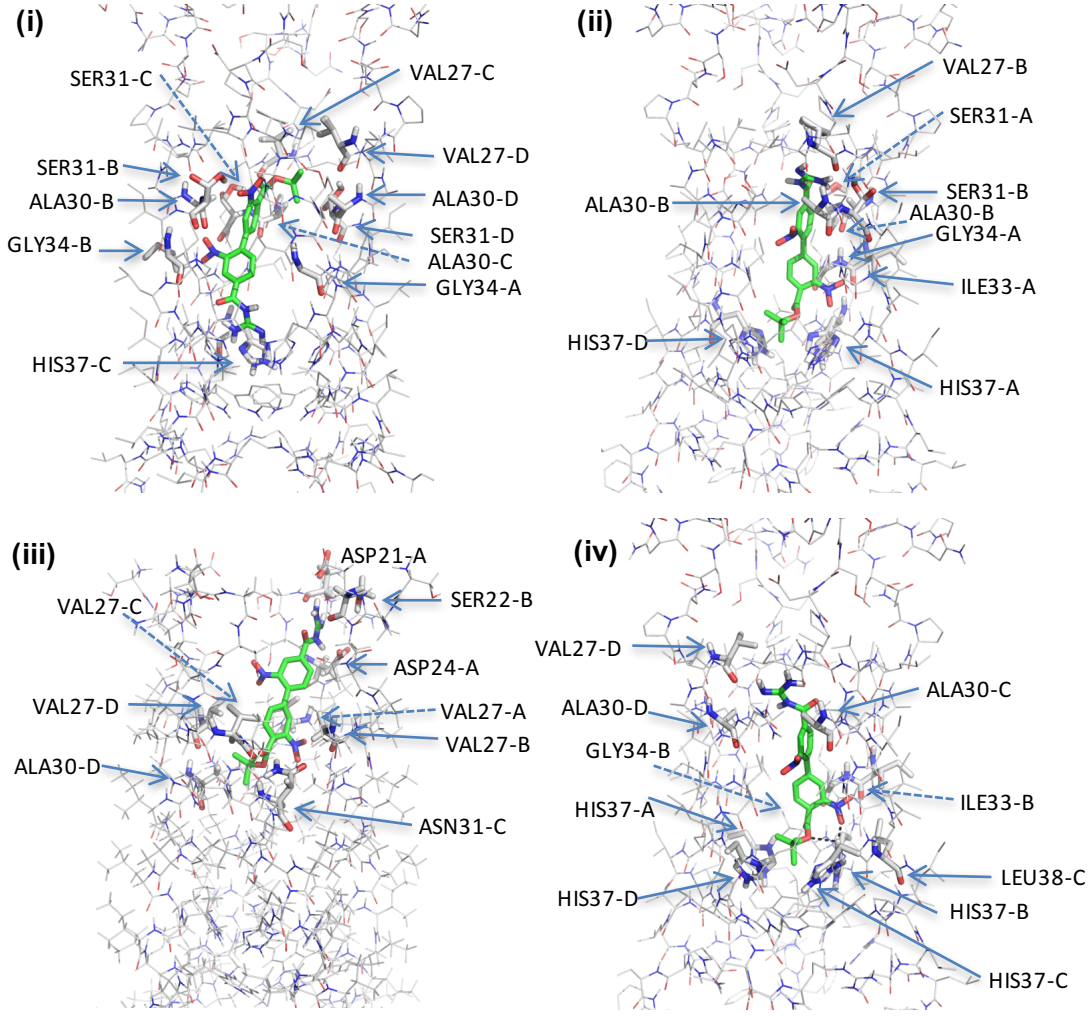

B

Compound 14

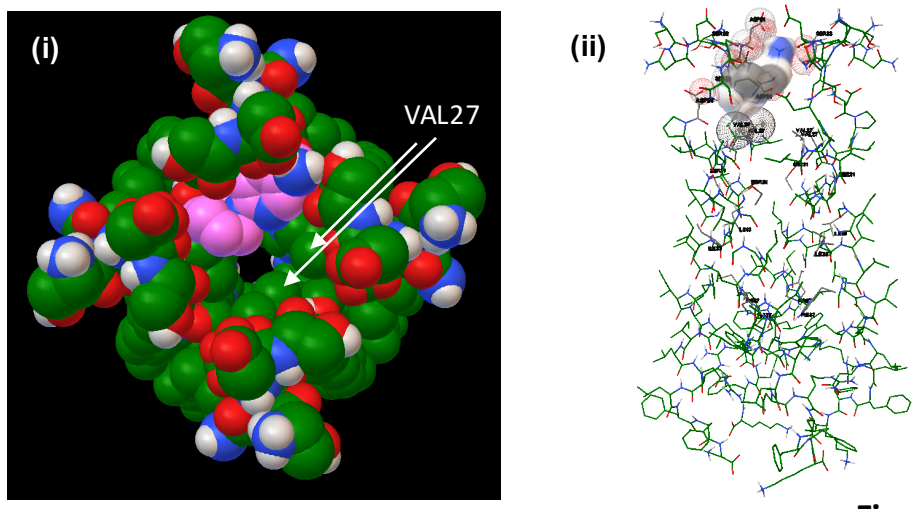

Figure 7